73rd International Astronautical Congress (IAC), Paris, France, 18-22 September 2022.

IAC–22–C1.6.10

A Transport Network for In-Orbit Recycling Exploiting Natural Dynamics

Maria Anna Laino[a]*, Andrew Ross Wilson[a], Massimiliano Vasile[a], Roberto Paoli[b], Catalin Gales[b]

[a]*Department of Mechanical & Aerospace Engineering, University of Strathclyde, James Weir Building, 75 Montrose Street, Glasgow, United Kingdom G11XJ*,
[b]*Department of Mathematics & Al. I. Cuza University of Iaşi, Blvd. Carol I, no. 11, 700506 Iaşi, Romania*
*Corresponding Author, maria.laino@strath.ac.uk

Abstract

This paper proposes an initial step towards the construction of a transport network connecting different orbit regimes with a Geosynchronous orbit in the Laplace plane and the Geosynchronous orbit with the Moon. This transport network will be designed to exploit a combination of natural dynamics and impulsive manoeuvres. The methodology proposed starts from the identification of regions, in orbital parameter space, around the Earth, where third-body effects concur to modify favourably the orbital elements. A sequence of manoeuvres is then devised to exploit these natural effects and achieve the desired final orbit. Conversely, the cislunar region will be connected thanks to impulsive manoeuvres and invariant manifolds, peculiar to the Circular Restricted Three-Body Problem. Finally, a perturbed two-body model is also used to identify possible disposal orbits for the decommissioned modular space assets.

Keywords: Geosynchronous Orbit, Orbital Transfers, Third-body Perturbations, Invariant Manifolds, Graveyard Orbit.

Nomenclature

G	Gravitational constant
L_i	Libration point
M	Mean anomaly
Ω	Right ascension of the ascending node
μ	Mass parameter
ω	Argument of perigee
θ	True anomaly
a	Semi-major axis
e	Eccentricity
i	Inclination
n	Mean motion
r_a	Apogee radius
r_p	Perigee radius
v	Velocity

Acronyms

AOP Argument Of Perigee

CORES COllaborative Recycling of End-of-life Sps

CR3BP Circular Restricted Three-Body Problem

DRO Distant-Retrograde Orbit

ECI Earth-Centered Inertial frame

GEO Geostationary Earth Orbit

GSO Geosynchronous Orbit

IADC Inter-Agency Space Debris Coord. Committee

LEO Low-Earth Orbit

NRHO Near-Rectilinear Halo Orbit

RAAN Right Ascension of the Ascending Node

SBSP Space-Based Solar Power

SPS Solar Power Satellite

TLE Two-Line-Element catalogue

1. Introduction

The disposal of large infrastructures in space, like a Solar Power Satellite (SPS), poses a considerable problem. This was discussed for the first time from a circular space economy perspective by [1] in a study which disclosed the findings of a comparative sustainability assessment on the space-based solar power (SBSP) concept with terrestrial-based energy generation options. A key finding from this was that very little literature on end-of-life operations of SPS systems exists, despite the relative importance of reducing resource dependency, energy intensity and the ecological footprint of the technology. The reason for this is due to the fact that modern SPS systems are envisaged to operate almost indefinitely, with proper repair and maintenance. Highly modular system concepts will allow individual elements of the satellite to be replaced on a regular basis. However, from both a technical and environmental perspective, this still raises two unanswered questions: how can flexible large-scale structures be autonomously constructed and dismantled in space and what happens to the decommissioned modular space assets at the end of life?

To address this problem, a project called CORES (COllaborative Recycling of End-of-life Sps) was recently initiated at the University of Strathclyde. CORES goes beyond the current effort to manage the space environment by removing space debris, avoiding collisions and de-orbiting space objects. It goes also beyond the simple in orbit servicing idea and looks at recycling and repurposing of space objects. In a way it follows in the footsteps of the Phoenix programme of DARPA [2], H2020 PERASPERA programme and aligns with the ESA OMAR programme but with specific application to SPS.

In this framework, there is the need to have frequent and low-cost transfers in Earth orbit and cis-lunar region. CORES aims at creating a continuous transport network between different orbital regimes to fetch and transport the parts of non-active satellites, that can be repurposed and used to remanufacture modular systems, like an SPS. The idea is to investigate regions in the phase space where natural dynamics plays in favour of the transfer. To do this, the orbital perturbations in Earth orbit and the already known pathways (like the manifolds in the Circular Restricted Three-Body Problem) will be mapped, in order to exploit them and facilitate construction in orbit. This work is focused on connecting a Geosynchronous orbit (GSO) in the Laplace plane with densely populated regions in space, as Low-Earth Orbit (LEO) and super-synchronous Graveyard orbit, and to the cis-lunar region, which will experience an increase in traffic in the upcoming years. The Laplace plane is a plane in which secular orbital evolutions due to lunisolar perturbation and Earth oblateness are zero, hence the orbits on this plane are frozen [3]. It has been proposed as a suitable location for a SPS [4], an alternative to the standard solution of a Geostationary Earth Orbit (GEO).

This paper proposes different transfer strategies used to connect the already cited orbital regimes, exploiting natural dynamics. Section 2 presents the LEO - GSO connection, a four-impulses transfer that uses the variation of orbital elements in a perturbed environment to gain in terms of delta-v. Section 3 describes the transfer strategy from a Halo orbit in the L_2 point of Earth - Moon system to the reference GSO. In this case, the invariant manifolds of the Circular Restricted Three-Body Problem are used to get as close as possible to Earth for free. Section 4 discusses disposal options by analysing the long-term evolution of the objects on super-synchronous orbits, under various perturbations, including the solar radiation pressure. In Section 5, the results concerning the previous sections are presented and discussed, and compared to the more classical results already in the literature. Lastly, the limitations of this work and the possible future extension are highlighted along with the conclusions, drawn in Section 6.

2. LEO - GSO Connection

In this work, the design of the orbital transfers from LEO to a GSO is based on a perturbed two-body problem, with the gravitational perturbation due to Earth oblateness and the third-body perturbations of the Sun and the Moon. In this case, the orbital elements are not constant, but they are a function of time. If we consider the direct two-impulses, half-ellipse LEO - GEO transfer in Fig. 1, the third-body perturbations acting on the orbit are small enough that the corresponding variation of the orbital elements is negligible, and the two-body approximation gives good estimates for the delta-v values required. But, when the apogee increases (as it is done in the bi-elliptic type of transfer), the effect of the third-body becomes increasingly more important. The orientation of the transfer orbits with respect to the Sun and the Moon - which depends on the epoch, Right Ascension of Ascending Node (RAAN) and Argument of Perigee (AOP) - and the timing of the manoeuvre are fundamental. These parameters control the variations in orbital elements on a transfer orbit, and their adequate selection may lead to a transfer in which the orbital elements vary in a such a way that the costs of the manoeuvres will be lower.

In particular, consider the classical bi-elliptic transfer in the two-body problem, or three-impulses transfer in Fig. 2. It consists in two half-elliptic orbits and three burns: the

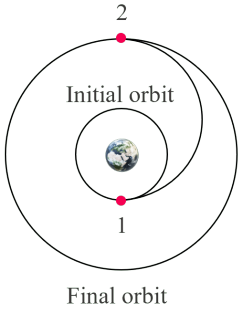

Fig. 1: Two-impulses transfer strategy. The numbers outline the sequence of the manoeuvres.

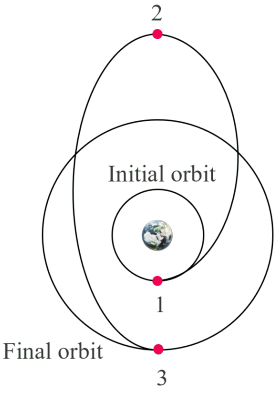

Fig. 2: Bi-elliptic transfer strategy. The numbers outline the sequence of the manoeuvres.

first one to enter an orbit with an apogee higher than that of a GSO, the second to change the inclination and enter an orbit with the perigee radius equal to that of a GSO, the last one to finally circularise the orbit. If the initial and final orbit have a different inclination i, the change of plane manoeuvre will be performed as far as possible from Earth where the velocity is lower (that is, at the apogee), being the cost of the manoeuvre (hereafter, "delta-v") $\Delta v = 2v \sin(\Delta i/2)$ [5]. In this case, Δi will always be constant and it will not depend on the propagation time of the orbit. If, however, we add the mentioned perturbations to the model, and let them act for a period of time, the inclination of the transfer orbit may vary thanks to the action of third-body perturbations [6, 7]. When the initial inclination is greater than the final one, the desirable effect of the perturbations would be to decrease the inclination, so that Δi is smaller. Furthermore, another effect that could be exploited is the variation of the radius of perigee, that should get as close as possible to the radius of a GSO. If we manage to exploit these effects, we can save in terms of delta-v compared to the classical and theoretical cases. The idea followed in this work is to map the variation in orbital elements caused by the perturbations in a certain time frame and establish what area of the phase space should be investigated.

In the proposed strategy, the geometry of the transfer is similar to that of a bi-elliptic transfer, but it consists in four burns instead of three, in which the change of plane and the change of perigee manoeuvres are located at different points. The first transfer orbit (or, the orbit prior to the plane change) is propagated up to time T, different from the semi-period or period of the orbit. The plane change manoeuvre is performed when the Δi is minimum, while the change of radius of perigee is performed at the subsequent apogee. Once on a GSO, the orbit is circularised with another manoeuvre, for a total of four impulsive manoeuvres.

2.1 The Perturbed Two-Body Problem

In the restricted two-body problem, two point masses move under their mutual gravitational attraction, with one of them (the spacecraft) being much smaller than the other (the Earth). The third-body perturbations of the Sun and the Moon, and the Earth oblateness are added to this model in the form of perturbing accelerations. The equations of motion in vector form are

$$\ddot{\mathbf{r}} = -\frac{G\,m}{r^3}\mathbf{r} + \mathbf{a}_{J_2} + \mathbf{a}_{Sun} + \mathbf{a}_{Moon} \tag{1}$$

where, G is the gravitational constant, m is Earth's mass, $\mathbf{r} = (x,\ y,\ z)$ is the position vector, x, y and z are the Cartesian coordinates in an Earth-Centered Inertial frame (ECI), see Fig. 3.The first term in Eq. (1) is the two-body acceleration term, while the other terms are, respectively, the accelerations coming from J_2, Sun and Moon gravity. The model described was implemented in MATLAB R2021b and validated with the software GMAT. The tolerance used in the integration process was set to 10^{-14}.

Given the fact that the dynamical system in Eq. (1) is conservative, an alternative approach involves the use of La-

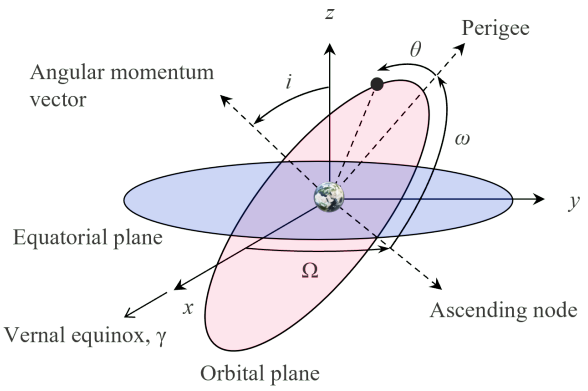

Fig. 3: ECI reference frame and orbital elements, see [5].

grange planetary equations (see [8])

$$\begin{aligned}
\frac{\mathrm{d}a}{\mathrm{d}t} &= \frac{2}{a\,n}\frac{\partial \mathcal{R}}{\partial M} \\
\frac{\mathrm{d}e}{\mathrm{d}t} &= \frac{\sqrt{1-e^2}}{e\,a^2 n}\left(\sqrt{1-e^2}\frac{\partial \mathcal{R}}{\partial M} - \frac{\partial \mathcal{R}}{\partial \omega}\right) \\
\frac{\mathrm{d}i}{\mathrm{d}t} &= -\frac{1}{a^2 n\sqrt{1-e^2}\sin i}\left(\frac{\partial \mathcal{R}}{\partial \Omega} - \cos i\frac{\partial \mathcal{R}}{\partial \omega}\right) \\
\frac{\mathrm{d}M}{\mathrm{d}t} &= n - \frac{2}{a\,n}\frac{\partial \mathcal{R}}{\partial a} - \frac{1-e^2}{e\,a^2 n}\frac{\partial \mathcal{R}}{\partial e} \\
\frac{\mathrm{d}\omega}{\mathrm{d}t} &= \frac{\sqrt{1-e^2}}{e\,a^2 n}\frac{\partial \mathcal{R}}{\partial e} - \frac{\cos i}{a^2 n\sqrt{1-e^2}\sin i}\frac{\partial \mathcal{R}}{\partial i} \\
\frac{\mathrm{d}\Omega}{\mathrm{d}t} &= \frac{1}{a^2 n\sqrt{1-e^2}\sin i}\frac{\partial \mathcal{R}}{\partial i}.
\end{aligned} \tag{2}$$

Here, $(a,\ e,\ i,\ M,\ \omega,\ \Omega)$ are the orbital elements, n is the instantaneous mean motion given by $n = \sqrt{Gm/a^3}$ and

$$\mathcal{R} = \mathcal{R}_{J_2} + \mathcal{R}_{Sun} + \mathcal{R}_{Moon}, \tag{3}$$

where $\mathcal{R}_{J_2}$, $\mathcal{R}_{Sun}$ and $\mathcal{R}_{Moon}$ are the disturbing functions due to the gravitational harmonic J_2, Sun and Moon, respectively. Following [9], we use a single-averaged model, obtained by averaging $\mathcal{R}$ over the mean anomaly M and expanding the third-body disturbing functions $\mathcal{R}_{Sun}$, $\mathcal{R}_{Moon}$ up to the tenth order in the paralax factor a/r_b, where r_b (with b = Sun or Moon) is the distance of the third body from the Earth. Orbit propagation with the averaged model is validated by comparison with the Cartesian approach. The accuracy and efficiency in the propagation of highly eccentric orbits using the method by Kaufman and Dasenbrock are discussed in detail in [10].

2.2 Methodology of the Transfer

The LEO - GEO transfer strategy proposed here follows the scheme represented in Fig. 4 and the dynamical model described by Eq. 1. The initial orbit is a circular orbit located in LEO, the final orbit is a circular GSO. The blue, green and yellow trajectories represent respectively the first, second and third transfer orbits. The numbers from one to four outline the sequence of the manoeuvres.

More in detail, the strategy consists of the following steps:

1. Imagine we have a spacecraft in an initial circular orbit in LEO, with radius $r_{p,i}$ and inclination i_i, that has to reach the desired final orbit, a circular GSO, with radius r_{GEO} and inclination $i_f < i_i$. It enters a first transfer orbit with a perigee radius $r_{p,i}$ and an apogee radius equal to $r_a > r_{\text{GEO}}$. To enter this orbit from the initial one a manoeuvre costing Δv_1 is needed (Manoeuvre 1).

2. The perturbations act on the first transfer orbit up to time T. Note that the initial orbital elements for the propagation are those in the previous point (the semi-major axis and eccentricity can be derived from $r_{p,i}$ and r_a), and the RAAN and AOP are fixed.

3. At time T, a change of plane manoeuvre (or change of inclination) is performed (Manoeuvre 2). This can happen only at two points along the orbit, exactly at the line of intersection of the two orbital planes. This translates into the condition on the true anomaly $\theta = 180\,\text{deg} - \omega$ and/or $\theta = 360\,\text{deg} - \omega$, which means that for it to happen at the apogee, the AOP should be $\omega = 0\,\text{deg}$ or $\omega = 180\,\text{deg}$. The variation of inclination of the change of plane manoeuvre is defined as $\Delta i = i_m - i$, where i_m is different from i_f. This is because along the second and third transfer orbits (green and yellow trajectories in Fig. 4) the inclination will change, so i_m is the inclination that will allow to have the final inclination exactly equal to the desired one. The delta-v relative to the plane change is Δv_2.

4. From the point of the second manoeuvre, the new transfer orbit is propagated up until the next apogee. Here, the third manoeuvre Δv_3 is performed so that the next perigee $r_{p,f}$ has a radius r_{GEO} and is on the desired GSO.

5. Once on the GSO, we perform a circularisation manoeuvre to enter a circular orbit (Manoeuvre 4). Final delta-v is Δv_4. The total delta-v is the sum of all four $\Delta v_t = \Delta v_1 + \Delta v_2 + \Delta v_3 + \Delta v_4$.

As explained in the premise of this section, we want to take advantage of the action of third-body perturbations from the Sun and the Moon to lower the costs of manoeuvre 2. This translates into having a smaller Δi than the one we would have without letting the perturbations act on the first transfer orbit for the time T. Hence, the variation of inclination over a fixed time interval (here fixed to a year) should be monitored, in order to find its minimum and establish where and when the change of plane manoeuvre should happen. The result of this process is the production of maps that record the *minimum variation of inclination* while varying all the parameters of the problem. In particular, the parameters that control the orientation of the transfer orbit with respect to the Sun and the Moon are the date of departure, initial RAAN Ω and AOP ω. The effect of third-body perturbations depends also on the size of the transfer orbit, meaning that if we fix the perigee $r_{p,i}$, the apogee radius r_a should be varied as well. Hence, the maps tell what are the parameters to choose in order to run the four-burns transfer strategy and compute the Δv_t.

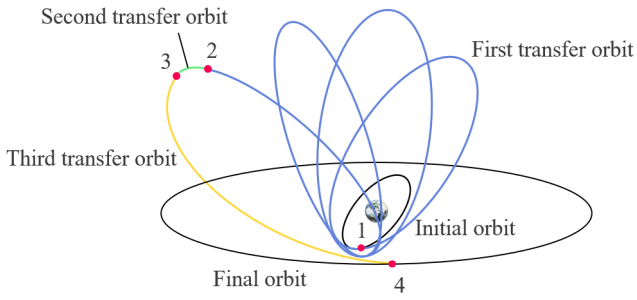

Fig. 4: Scheme of the LEO - GSO transfer strategy.

3. Moon - GSO Connection

In the last few years, the interest in visiting and studying the Moon has grown enormously. Also, the idea of manned exploration has become popular with the concept of the Lunar gateway among the others - a small space station intended to orbit a Near-Rectilinear Halo Orbit (NRHO) about Lagrange point L_2 of the Earth-Moon system [11]. The Lagrange points are advantageous locations for space missions, in particular Earth-Moon L_2 could serve as a gateway to other destinations in the Solar System, or it could be used as a communication link between the Earth and the hidden side of the Moon [12]. As this location will be more and more crowded in the future, it was decided to try to connect it with our desired GSO orbit in the Laplace plane. The literature on the topic proposes different transfer strategies to link Earth-Moon L_2 and Earth orbit [13, 14]. A first possibility would be to use a more classical direct transfer (like a Hohmann transfer), already proven in the past but among the most fuel-consuming methods. Another strategy would be to employ the invariant manifolds structures associated to periodic orbits in a three-body system, see the Genesis mission profile in Earth-Sun system [12]. In the case of Earth-Moon, the manifolds associated to Halo orbits do not approach the GSO directly, but they can be used to travel to the vicinity of Earth in a cheap way. Another transfer approach is the one used by the Hiten mission [15]. It employed the *weak stability boundaries* transfer strategy, which accounts for two patched three-body problems (Earth-Moon and Earth-Sun in this case), and requires a more complicated design.

The strategy proposed to transfer from the vicinity of the Moon to the desired GSO through an invariant manifold is explained in the following, starting from the peculiar dynamics in the Earth-Moon system.

3.1 The Circular Restricted Three-Body Problem

The Circular Restricted Three-Body Problem (CR3BP) describes the motion of a smaller body under the gravitational attraction of two massive bodies in a circular, coplanar motion around their common centre of mass. This model is used here to describe the motion of a spacecraft in the Earth-Moon system. This motion is better described in a rotating reference frame, centered at the centre of mass of the system, with x-axis always directed towards the Moon, z-axis aligned with the angular momentum vector of Earth and Moon and y-axis completing the triad, see Fig. 5. The motion of the spacecraft is governed by the following equations

$$\begin{aligned} \ddot{x} - 2\dot{y} &= -\frac{\partial \bar{U}}{\partial x} \\ \ddot{y} + 2\dot{x} &= -\frac{\partial \bar{U}}{\partial y} \\ \ddot{z} &= -\frac{\partial \bar{U}}{\partial z} \end{aligned} \tag{4}$$

which are normalised using the characteristic quantities of the Earth-Moon system. In particular, the characteristic length, velocity and time are respectively 3.850×10^5 km, 1.025 km/s and 2.361×10^6 s, taken from [16]. $\bar{U}$ is the effective potential of the system, expressed as

$$\bar{U} = -\frac{1}{2}\left[(1-\mu)r_1^2 + \mu r_2^2\right] - \frac{1-\mu}{r_1} - \frac{\mu}{r_2} \tag{5}$$

where

$$r_1 = \sqrt{(x+\mu)^2 + y^2 + z^2}$$
$$r_2 = \sqrt{(x-1+\mu)^2 + y^2 + z^2}$$

which are, respectively, the distances of the spacecraft from Earth and Moon. μ is the mass parameter, that is the ratio of the mass between the smaller primary (the Moon in our case) and the total mass of the system. For the Earth-Moon system, $\mu = 0.01215$.

Eq. 4 admits five equilibrium solutions, called *Lagrange points* or *libration points* L_i. As shown in Fig. 5, the points L_1, L_2 and L_3 lie on the x-axis of the rotating frame and are called *collinear points*, while L_4 and L_5 lie on the vertex of an equilateral triangle. Different families of periodic and quasi-periodic orbits exist about the Lagrange points [17, 18, 19]. Halo orbits are three-dimensional periodic orbits that generate around the collinear points. Halo orbits about the same point are divided into *southern* and *northern* families, symmetrical with respect to the xy-plane. "Northern" means that the maximum out-of-plane amplitude A_z of the orbit is in the $+z$ direction, "southern" means it is in the $-z$ direction. Halo orbits can be univocally defined by their family (northern or southern) and their amplitude A_z. In this work, Halo orbits were generated by using a third-order approximation developed by Richardson [20] as first guess, refining it with a differential correction process, explained more in detail in the work by Howell [21].

Another feature of the CR3BP is the existence of the invariant manifolds associated with the points L_1 and L_2 and with their periodic orbits [22]. These manifolds, also referred to as manifold "tubes", provide solutions for the design of low-energy spacecraft trajectories, connecting different realms of a three-body system. In short, stable/unstable manifolds are phase space structures consisting of all the vectors whose future/past positions converge to the orbit. Hence, if a spacecraft is on a stable manifold, its trajectory will wind onto the orbit, while if it is on the unstable one, it will wind off of it. The procedure that was used in this work to obtain invariant manifolds is cumbersome and requires dynamical system tools. It follows the work by Koon et al. [16], which is advised for a more detailed discussion on the topic. The model and structures described here were implemented in MATLAB R2021b and validated with the software GMAT. The tolerance used in the integration process was set to 10^{-11}.

3.2 Methodology of the Transfer

In this work, only Halo orbits about the L_2 points were considered, but the analysis can be easily extended to L_1 as well. The transfer strategy used to connect a L_2 Halo orbit

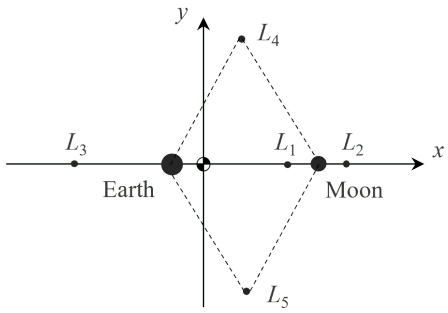

Fig. 5: The rotating frame of the CR3BP and the location of the five Lagrange points.

in the Earth-Moon system and our reference GSO circular orbit is shown in Fig. 6. The numbers from one to three outline the sequence of the manoeuvres. The strategy simply consists in the following steps:

1. N unstable manifolds are generated from N points on a northern Halo orbit with fixed out-of-plane amplitude A_z. They are propagated for a maximum time T. The cost of leaving the Halo orbit (point 1 in Fig. 6) can be approximated as zero, as they are always lower than $1\,\mathrm{m/s}$ [14], opposed to the costs of the other manouvres (in the order of $\mathrm{km/s}$).

2. All the intersections of the manifolds with the plane that contains the final GSO (that is, the averaged Laplace plane) are recorded. Of all of them, the intersection point closer to Earth is saved (point 2 in Fig. 6). The Laplace plane is defined in the ECI reference frame, so a transformation between this frame and the CR3BP rotating frame is needed to meet the condition. For the sake of simplicity, the orbit of the Moon about Earth was considered to be circular and with a constant inclination.

3. A Lambert problem [5] (defined in the two-body problem) is used to connect this last point to the circular GSO in the Laplace plane. The Lambert problem consists in determining an orbit from two position vectors and the time of flight between them. To employ this method, the time spent on the arc and the entrance point on the final orbit (point 3) must be fixed. At point 2, the first delta-v Δv_2 is computed.

4. A manoeuvre is performed to enter the GSO. The cost of this manoeuvre is Δv_3. The total cost of this transfer strategy is then $\Delta v_t = \Delta v_2 + \Delta v_3$.

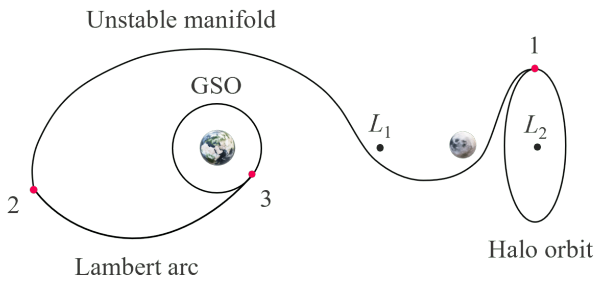

Fig. 6: Scheme of Moon - GSO transfer strategy.

4. GSO - Graveyard orbit Connection

At the end of its life, a decommissioned modular space asset should be transferred from GSO to a super-synchronous orbit that does not cross the GEO protected region for at least 100 years (see [23]).

If for the LEO - GSO connection and the Moon - GSO connection, the methodology discusses "how" to transfer from a given region to GSO, in the case of the GSO - Graveyard orbit connection the question is "where" the object should be moved at the end of its life. In the following, we discuss some disposal options, analyse the long-term evolution on super-synchronous orbits under various effects and propose a methodology of determining graveyard orbits.

A disposal orbit can be established after analysing the long-term effects induced by all perturbations, including the influence of the solar radiation pressure. By fulfilling the following two conditions, the Inter-Agency Space Debris Coordination Committee (IADC) assesses that the orbit remains above the GEO protected region for a long interval of time (see [23]):

1. A minimal increase in the perigee altitude of

$$235\ \text{km}\ + 1000\, C_r\, \frac{A}{m}\,, \tag{6}$$

   where C_r is the solar radiation pressure coefficient, typically in the range of about 1.2 to 1.5, A/m is the area to mass ratio in m^2/kg.

2. An eccentricity less than 0.003.

Other options exist and in all situations a detailed analysis of the dynamics should be performed to guarantee that the graveyard orbit will not interfere with the GEO protected region for at least 100 years.

The strategy to transfer from GSO to a disposal orbit involves a priory determination of the graveyard regions that fulfil the IADC requirement according to which the orbits are not crossing the GEO protected region. The averaged model defined by Eq. (2) and Eq. (3) and described in Section 2.1 allows to perform a fast and accurate analysis of the dynamics on secular time scales.

4.1 Orbital evolution on super-synchronous orbits

This Section characterizes the long-term evolution of the known objects revolving around the Earth on super-synchronous orbits. According to the Two-Line-Element catalogue (see [24]), hereafter TLE, there are more than 350 objects orbiting on super-synchronous trajectories. Fig. 7 and Fig. 8 report the variation of radial distance as a function of the semi-major axis and respectively the variation of inclination as a function of the initial inclination of the orbits of this population, over a fixed interval of time T, where $T = 0$ years (top left), $T = 20$ years (top right), $T = 50$ years (bottom left) and $T = 100$ years (bottom right). Since the value of the A/m parameter is set to zero in the two-line element set for this population (see [23]), each orbit is propagated without considering the influence of the solar radiation pressure.

The top left panel of Fig. 7 shows that there are more than 20 objects with perigee lower than the altitude of the GEO protected region. In the absence of the solar radiation pressure, since the orbital motion of this population is not influenced by luni-solar secular resonances (see [25, 26, 27] for the location of luni-solar resonances) the secular evolution of the radial distance remains in the limits imposed by the initial conditions. Fig. 8 shows that inclination vary over secular times, a phenomenon well know from 60's (see [28]).

4.2 Effect of solar radiation pressure

For objects with moderate to high area-to-mass ratio, the solar radiation pressure effect is non-negligible. The main effect of solar radiation pressure is to produce long-term variations of the eccentricity and inclination. The amplitude and period of these variations depend on the initial conditions of the given object and on its area-to-mass ratio.

We remark that objects in the graveyard region must have a limited value of the area-to-mass ratio because of condition 1. from the previous section. However, it is important to assess the evolution of orbits of objects with high area-to-mass ratio. For instance, it could be used to describe the dynamics of a spacecraft equipped with a solar sail interacting with the debris in the GEO graveyard region, but also to assess the threat of a particularly large piece of debris which found itself in the graveyard region after a catastrophic event.

From [29] we know that a GEO object with high area-to-mass ratio in an almost circular orbit is subjected to a

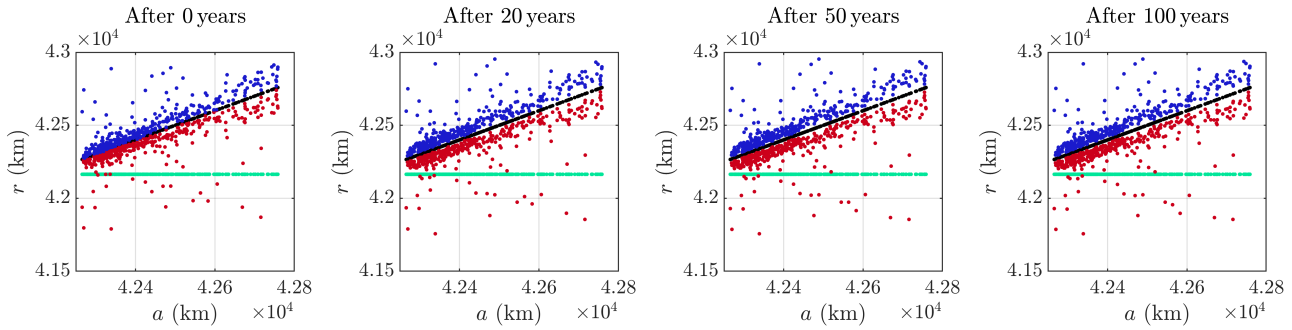

Fig. 7: Radial distance variation for the objects from the TLE catalogue ($A/m = 0\,\mathrm{m}^2/\mathrm{kg}$), orbiting on super-synchronous trajectories. Each object is represented by three coloured points, marked in black, blue and red, where the black point gives the value of the semi-major axis, the red one provides the minimum perigee radius reached over the propagation time, while the blue point corresponds to the maximum apogee radius reached over the time span. The horizontal green line marks the location of the geostationary ring.

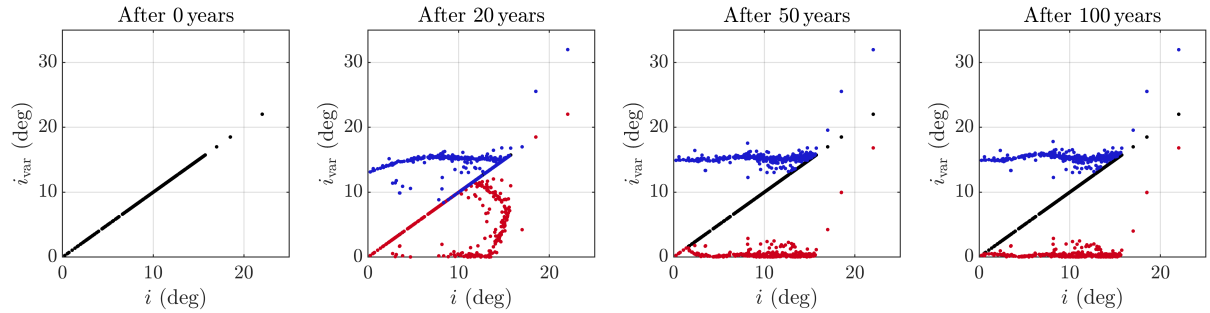

Fig. 8: Inclination variation of the super-synchronous orbits of the objects from the TLE catalogue, $A/m = 0\,\mathrm{m}^2/\mathrm{kg}$. Excluding the top left plot, in each panel, each object is represented by three coloured points, marked in black, blue and red, where the black point gives the value of the inclination at initial time, the red one provides the minimum inclination reached over the propagation time, while the blue point corresponds to the maximum inclination reached over the time span.

yearly variation of the eccentricity, whose amplitude is proportional to the square root of the area-to-mass ratio, ranging from a maximum eccentricity of 0.1 if $A/m = 5\,\mathrm{m}^2/\mathrm{kg}$ to a maximum eccentricity of 0.4 if $A/m = 20\,\mathrm{m}^2/\mathrm{kg}$.

As far as the inclination is concerned, the maximum deviation from an equatorial orbit is of $45\,\mathrm{deg}$, but the period of such variations is inversely proportional to the square root of the area-to-mass ratio. An object with an high value of the *effective area-to-mass ratio* $C_r\,A/m$ such as $10\,\mathrm{m}^2/\mathrm{s}$, in an equatorial orbit around Earth ($i = 0\,\mathrm{deg}$) will reach the inclination of the Laplace plane in GEO in roughly five years. Fig. 9a and Fig. 9b show the evolution of the semi-major axis, eccentricity and inclination of the objects in the TLE catalog, assuming that all have the same area-to-mass ratio. Fig. 9a describes the initial state of the TLE catalog and it was obtained by propagating the orbits of all available objects to a common epoch. Fig. 9b describes the distribution of the orbital elements $(a,\, e,\, i)$ after propagating all objects assuming they have all the same area-to-mass ratio, equal to $5\,\mathrm{m}^2/\mathrm{kg}$. As predicted by Valk [29], we can appreciate a yearly variation of the eccentricity and also notice that all objects are slowly but steadily increasing the inclination. We conclude by noticing that the only way of facilitating the connection from the graveyard region to the GSO is to use a large solar sail, as doing so will diminish the time necessary to reach the required connection.

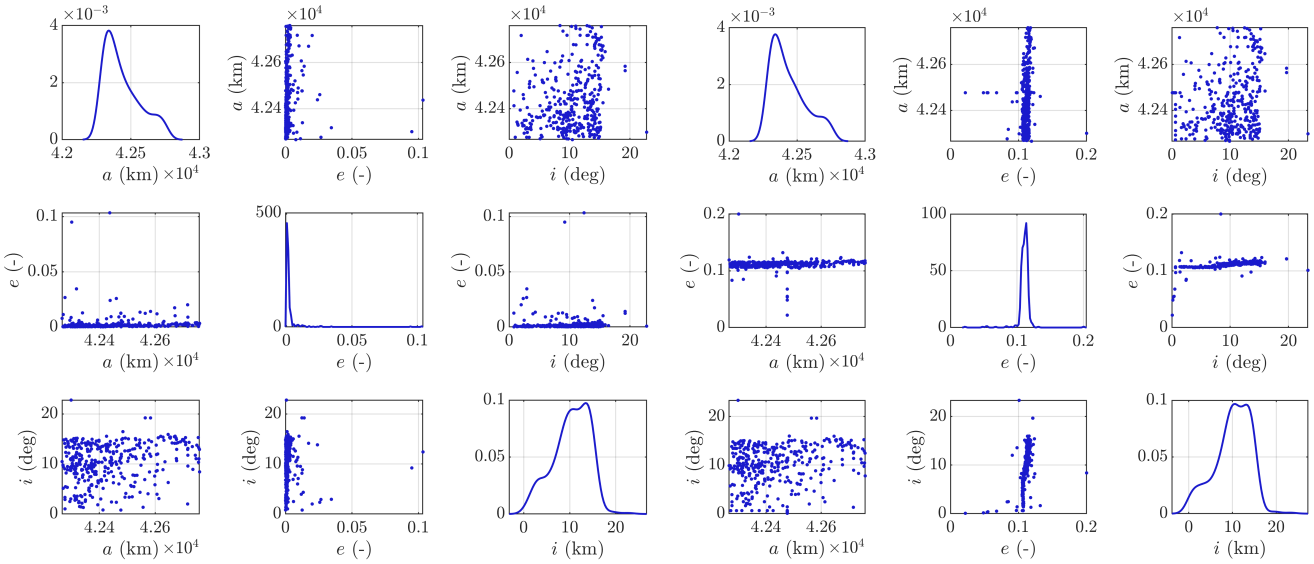

(a) Initial distribution.

(b) Distribution after six months.

Fig. 9: Distribution of the orbital elements (a, e, i) from the TLE catalog.

4.3 Determination of graveyard orbits

The methodology of determining graveyard orbits consists in evaluating the eccentricity and inclination growth over a period of 100 years. In this respect, the averaged model, defined by Eqs (2), (3), in which the influence of the solar radiation pressure is also considered, is used to propagate orbits characterized by various parameters. To analyse the IADC conditions mentioned above and also to explore other options, we proceed as follows:

1. We propagate a set of 500 orbits, for which we fix the initial eccentricity and inclination and vary the A/m parameter in the range of $0\,\mathrm{m}^2/\mathrm{kg}$ to $1\,\mathrm{m}^2/\mathrm{kg}$. For each value of A/m, from the formula (6), we determine the initial perigee and hence the initial semimajor axis. The other initial orbital elements, that is the angles, are taken at random in the interval $(0,\ 360)$ deg.

2. For each orbit we record the minim perigee and maximum apogee reached over a given interval of time T and evaluate whether the orbit crosses the GEO protected region (-200 km below and $+200$ km above the geostationary ring).

3. We also record the minimum and maximum values of the inclination reached over time T.

5. Results

This Section reports the results relative to the methodologies outlined in Sections 2, 3 and 4. The results are analysed and discussed. Limitations and future extensions are explored as well.

5.1 LEO - GSO Connection

Here, the results obtained following the procedure of Section 2 are reported. The inclination of the targeted GSO is equal to $i_f = 7.4\,\mathrm{deg}$, which is the inclination of the averaged Laplace plane [3]. The minimum variation of inclination Δi was mapped over the time span of a year varying all the cited initial parameters: initial inclination i_i, initial AOP and RAAN, radius of perigee of the initial orbit, radius of apogee of the first transfer orbit r_a and departure date. A total of 112 maps were generated with:

- Four initial inclinations $i_i = (30,\ 60,\ 90,\ 120)$ deg.
- An initial radius fixed to $r_{p,i} = 7500\,\mathrm{km}$.
- A $360\,\mathrm{deg} \times 360\,\mathrm{deg}$ grid with $2\,\mathrm{deg}$ step for both the AOP and the RAAN.
- Four radii of apogee for the first transfer orbit $r_a = (1.5,\ 3,\ 5,\ 7) \times 10^5\,\mathrm{km}$.

- Seven departure dates: noon of $14/3/2023$, $21/3/2023$, $28/3/2023$, $4/4/2023$, $21/6/2023$, $23/9/2023$ and $22/12/2023$.

The propagation is stopped if the radius of the perigee gets smaller than the equatorial radius of the Earth or if the Moon is crossed. In that case, the information up to that point is saved. The first maps in Fig. 10 (first column) show the *minimum* variation in inclination over the time span of a year for $i_i = 60\,\mathrm{deg}$, $r_{p,i} = 7500\,\mathrm{km}$, r_a = $300\,000\,\mathrm{km}$ and three departure dates. The other maps in the figure (respectively, second, third and fourth columns) show the radius of perigee, propagation time and AOP recorded at the time the minimum Δi is reached. Up to $300\,000\,\mathrm{km}$, these maps can be obtained using Eq. (2), as this method is faster compared to the propagation using the full Cartesian form of Eq. (1), and the difference in numbers is small. Hence, this method can be used up to a certain altitude to analyse the full parameter space, with a $360\,\mathrm{deg} \times 360\,\mathrm{deg}$ grid in AOP and RAAN, in order to understand the overall behaviour of orbital elements. In the case a more refined analysis is needed or the transfer orbits have farther apogees, it is advised to use the full Cartesian form to obtain the maps.

As previously mentioned, the orientation of the transfer orbits with respect to the Sun and the Moon depends on the departure date. That is why many different dates were analysed: four of them following the position of the Sun in a whole year ($21/3/2023$, $21/6/2023$, $23/9/2023$ and $22/12/2023$), four of them following the position of the Moon during its orbital period ($14/3/2023$, $21/3/2023$, $28/3/2023$ and $4/4/2023$). As it can be noted, Fig. 10a and Fig. 10b, about only 20 days apart, show small differences in numbers and patterns, which can be attributed to the motion of the Moon. The maps in Fig. 10c, instead, are six months distant and are consistently different from the previous ones, as the Sun is in a new position.

From here, one must decide what is the area in the maps that should be explored to find transfers with a lower delta-v. As explained in Section 2, the change of plane manoeuvre should happen as far as possible from the central body, translating into having the AOP of the orbit at the manoeuvring point (that is, when Δi is minimum) as close as possible to $0\,\mathrm{deg}$ or $180\,\mathrm{deg}$ (ω_f in the maps). This means it would not be efficient to analyse the whole parameter space, one should instead restrict the search around those areas. In this work, the search was restricted only to the vicinity of $\omega_f = 180\,\mathrm{deg}$, as obtaining the maps using the full Cartesian equations requires a long computational time. Fig. 11 shows the detail of two of the maps in Fig. 10, this time refined using the full Cartesian model.

From these refined maps, the delta-v s corresponding to the strategy of Section 2 were computed, see Fig. 12. The first map of the three reports the total delta-v, the others show the costs for the second (change of plane) and third (change of perigee) manoeuvres of the strategy in Fig. 4. The white areas are referred to the areas in the maps in Fig. 11 that do not show a favourable variation in Δi (darker red, means that for those initial conditions the inclination is increasing instead of decreasing). Furthermore, when there was a close passage with the Moon resulting in an eccentricity bigger than one, the result was discarded. The computation was limited to a ω_f in the range $(170,\ 190)\,\mathrm{deg}$. It can be noticed how the Δv_2 map follows the pattern of ω_f and shows the very minimum where Δi gets smaller, while the Δv_3 follows the perigee and gets smaller as r_p increases.

The delta-v s corresponding to *all* the 112 maps were computed and saved. Fig. 13 shows all of them against the radius of apogee of the first transfer orbit for the four initial inclinations. They were compared with with the delta-v s of the theoretical transfers in a two-body problem: two-impulses transfers (in Fig. 1), bi-elliptic transfers (in Fig. 2) and bi-parabolic transfers, that are bi-elliptic transfers with the change of plane manoeuvre at infinite. The values of these theoretical delta-v s are reported in Table 1. It must be underlined how these transfer are not applicable in a perturbed environment, but their values are given anyway to give an idea of the numbers involved. The vertical dashed line in Fig. 13 represents the two-impulses theoretical value, the dashed-dotted line is the theoretical limit of a bi-parabolic transfer and the solid coloured lines are bi-elliptic theoretical values. From Fig. 13, one can draw the following conclusions:

- For an initial inclination $i = 30\,\mathrm{deg}$, the figure says that the theoretical two-impulses strategy is always the best option. This means that the difference in delta-v spent to reach an apogee farther than a GEO is always bigger than what we gain with a favourable action of the perturbations. Also, when the change in inclination is greater than $\sim 39.9\,\mathrm{deg}$, two-impulses transfer are always cheaper than bi-elliptic transfers [6, 7]. On a simple half-ellipse from LEO to GEO the third-body perturbations can be considered small enough that the two-body approximation gives good estimates of the actual costs, so this theoretical result can be considered reliable in this case as well.

- From $i = 60\,\mathrm{deg}$ we start to see how the strategy proposed here outperforms the theoretical ones. For all the initial apogees we can find solutions with lower costs than the two-impulses strategy. As the initial apogee increases, the minimum delta-v obtained gets

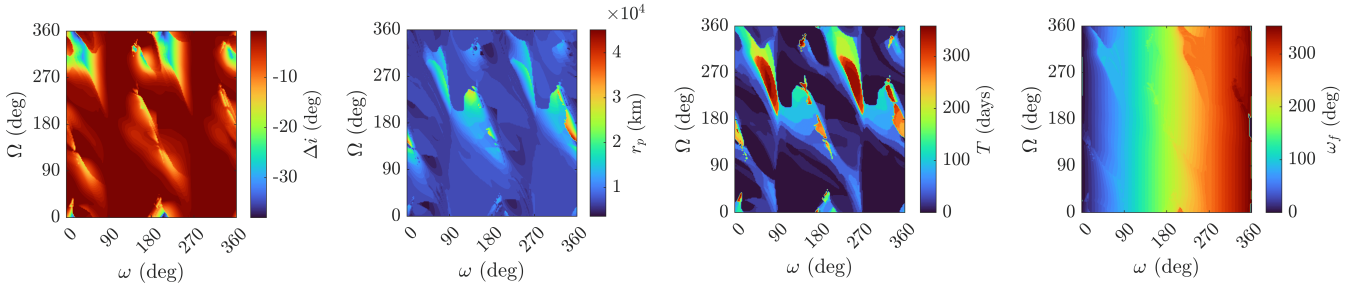

(a) Departure date $14/3/2023$.

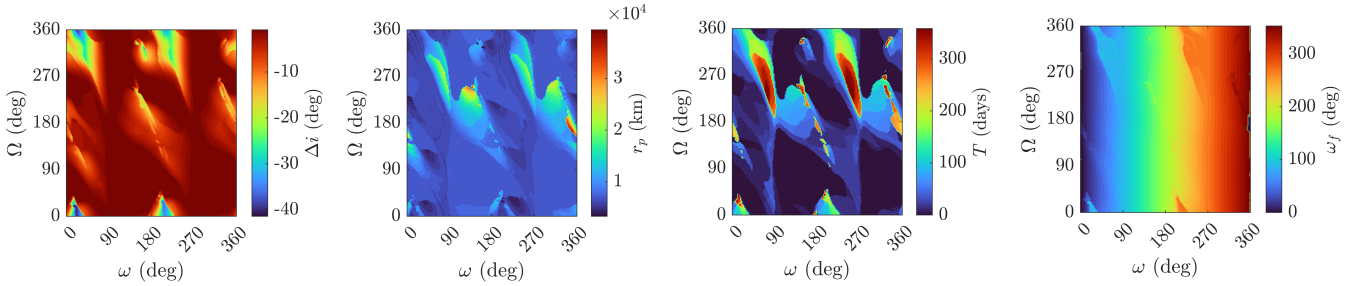

(b) Departure date $4/4/2023$.

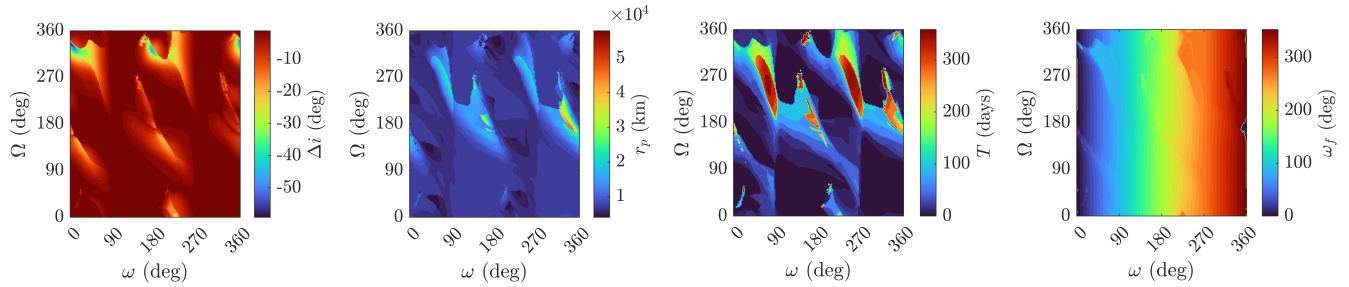

(c) Departure date $23/9/2023$.

Fig. 10: Maps for initial conditions $i_i = 60\,\text{deg}$, $r_{p,i} = 7500\,\text{km}$ and r_a = 300 000 km and three different departure dates. The first map records the minimum variation in inclination. The other maps report respectively the radius of perigee, propagation time and AOP recorded *at* the minimum Δi point.

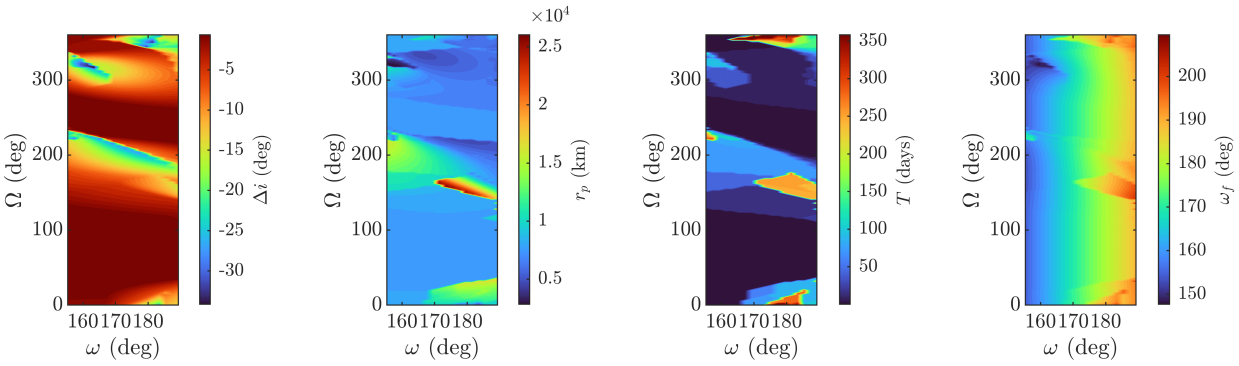

(a) Departure date $4/4/2023$.

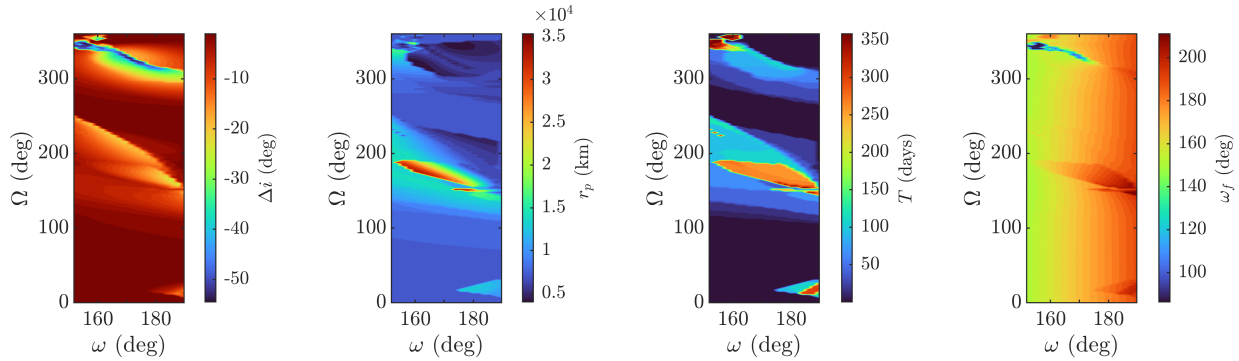

(b) Departure date $23/9/2023$.

Fig. 11: Restricted maps for initial conditions $i_i = 60\,\text{deg}$, $r_{p,i} = 7500\,\text{km}$ and $r_a = 300\,000\,\text{km}$ and two different departure dates. The first map records the minimum variation in inclination. The other maps report respectively the radius of perigee, propagation time and AOP recorded *at* the minimum Δi point.

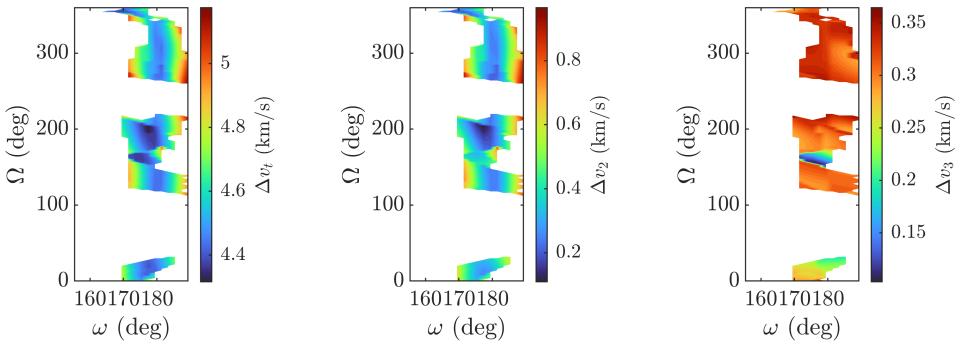

(a) Departure date $4/4/2023$.

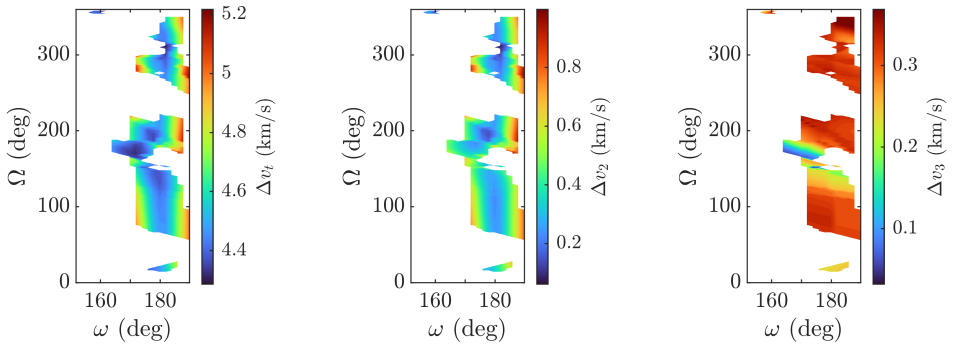

(b) Departure date $23/9/2023$.

Fig. 12: Delta-v maps for initial conditions $i_i = 60\,\mathrm{deg}$, $r_{p,i} = 7500\,\mathrm{km}$ and r_a = 300 000 km and two different departure dates. The first map of the three reports the total delta-v, the others show the costs for the second and third manoeuvre of the strategy, respectively.

smaller, overtaking the bi-elliptic values and even the bi-parabolic theoretical limit of $4.2921\,\mathrm{km/s}$.

- Similar considerations can be drawn for the $i = 90\,\mathrm{deg}$ and $i = 120\,\mathrm{deg}$ cases. It seems more convenient to raise the apogee farther than $150\,000\,\mathrm{km}$ to have a considerable gain over the bi-elliptic cases. For greater inclinations, the delta-v is generally bigger compared with the $i = 60\,\mathrm{deg}$ case, which is reasonable as in this case, even with the action of perturbations, the Δi will still be larger. Looking at Table 1, though, we can affirm that the higher is the inclination, the higher are the savings.

Fig. 14 shows a detail of Fig. 13 with the solutions that outperform the bi-elliptic theoretical values, Fig. 15 reports some of these solutions (for $i = 60\,\mathrm{deg}$ and two departure dates) in the (ω, Ω) plane. From these figures one could draw the conclusions that raising the apogee to $150\,000\,\mathrm{km}$ and let the perturbations act for a certain time period is *never* convenient. This is wrong, as we are comparing our strategy with an ideal case, that does not take into account the presence of perturbations. In the case of a perturbed environment, the theoretical bi-elliptic transfer would not be applicable anymore. We can suppose that, if the manoeuvre were to be performed exactly at $150\,000\,\mathrm{km}$, this would not be at the apogee anymore, but at a different point due to the action of perturbations, meaning it would require a larger delta-v than the theoretical one, and making our strategy more convenient. This aspect will require a further future analysis.

An important consideration is related to the times of flight involved in the proposed transfers. As already explained, the perturbations are allowed to act for a maximum of a year, to then find in this time interval the minimum variation of inclination Δi, in correspondence of which the change of plane manoeuvre should be performed. This implies that the total transfer times could be long, even more than a year. Tables 2, 3 and 4, show the time of flight and the number of revolutions relating to the minima in Fig. 14 to give an idea of the numbers involved. As it can be noticed, the ΔT associated with these results ranges from about 14 days to more than a year, against the direct two-impulses transfers that require larger costs (see Table 1) but transfer times of about 10 hours, a considerably lower data. In this case, it is necessary to make a trade-off between the gain on manoeuvring costs and the increase of the transfer times. For certain, the strategy proposed here will not be convenient for commercial transfers that need to have a perfectly working service just a few days after launch, but it could be convenient when many pieces of non-operational satellites have to be transported for a planned, non-urgent re-manufacturing of an SPS (see the Introduction).

The transfer strategies proposed in this paper offer advantages as they outperform the classical transfer types in terms of delta-v just with the help of natural dynamics, though having the clear disadvantage of requiring longer transfer times. Another limit could be given by the fact that the action of third-body perturbations, and therefore the possibility of saving or not, strictly depends on the time of the year, or, on the specific date of departure, meaning that our strategy lacks the flexibility in the launch of a direct two-impulses transfer. A future extension to this work will have to explore more initial parameters in order to draw more general conclusions. Another interesting analysis involves the variation and optimisation of the number and sequence of burns required to move from a LEO to a GSO. Finally, it would be useful to extend this analysis to the case of a LEO-GSO transfer that exploits low-thrust propulsion [30].

5.2 Moon - GSO Connection

The results obtained following the procedure in Section 3 are reported in the following. The orbit of the Moon about the Earth is very complicated, so the assumptions made previously are still considered valid. Its inclination varies in between $\sim 18\,\mathrm{deg}$ and $\sim 29\,\mathrm{deg}$ [31], for the sake of simplicity in this work it was considered fixed to $i = 18.28\,\mathrm{deg}$. The unstable manifolds departing from the L_2 northern Halo were propagated for a maximum of $T = 6\,\mathrm{months}$. $N = 1000$ manifolds were generated from as many points on the orbit. A total of 20 different Halo orbits were analysed, with amplitude A_z varying from $1000\,\mathrm{km}$ to $20\,000\,\mathrm{km}$, with a $1000\,\mathrm{km}$ step. As a reference, 10 manifolds propagated for 6 months from a Halo with amplitude $A_z = 20\,000\,\mathrm{km}$ are represented in Fig. 16.

Once found the crossing point with the Laplace plane closer to Earth, a Lambert arc was used to link it to our target circular GSO with inclination $i = 7.4\,\mathrm{deg}$. To employ a Lambert problem, the time of flight ΔT on the arc and the entrance point (defined as an angle, θ) on the final orbit (point 3 in Fig. 6) must be fixed. Here, for each of the 1000 points related to the 20 orbits, a range of values were analysed with:

- ΔT going from $10\,\mathrm{hours}$ to $10\,\mathrm{days}$ with a $4\,\mathrm{hours}$ step.
- θ varying from $0\,\mathrm{deg}$ to $360\,\mathrm{deg}$ with a $1\,\mathrm{deg}$ step.

The map in Fig. 17, containing the total cost associated with this method, was generated for all the parameters analysed.

From each map, the very minimum was found employing MATLAB's fmincon function, using the minimum in

Apogee (km)	Δv for $i = 30\,\mathrm{deg}$ (km/s)	Δv for $i = 60\,\mathrm{deg}$ (km/s)	Δv for $i = 90\,\mathrm{deg}$ (km/s)	Δv for $i = 120\,\mathrm{deg}$ (km/s)
42 241 (GEO)	3.8581	4.6576	5.5193	6.2436
150 000	4.1826	4.4088	4.6685	4.8928
300 000	4.2402	4.3531	4.4847	4.5992
500 000	4.2618	4.3294	4.4088	4.4781
700 000	4.2707	4.3190	4.3758	4.4255
Infinite	4.2921	4.2921	4.2921	4.2921

Table 1: Theoretical delta-v s for two-body problem transfers. The first row refers to a classical two-impulses transfer, the last row to a bi-parabolic transfer and the rest refer to bi-elliptic transfers with different radius of apogee.

Apogee (km)	Δv (km/s)	ΔT (days)	Nr. revolutions
150 000	4.49	264.35	106
300 000	4.29	97.42	16
500 000	4.19	14.20	2
700 000	3.81	59.08	3

Table 2: Minimum delta-v s for $i = 60\,\mathrm{deg}$ with the associated total propagation time and number of revolutions.

Apogee (km)	Δv (km/s)	ΔT (days)	Nr. revolutions
150 000	4.73	279.65	113
300 000	4.45	362.69	54
500 000	4.27	13.42	2
700 000	3.87	58.68	4

Table 3: Minimum delta-v s for $i = 90\,\mathrm{deg}$ with the associated total propagation time and number of revolutions.

Apogee (km)	Δv (km/s)	ΔT (days)	Nr. revolutions
150 000	4.91	267.04	109
300 000	4.55	270.47	40
500 000	4.39	41.14	4
700 000	3.80	386.89	17

Table 4: Minimum delta-v s for $i = 120\,\mathrm{deg}$ with the associated total propagation time and number of revolutions.

the map as the initial point in the procedure, with the constraints respecting the previous ranges on ΔT and θ. All the results are reported in Fig. 18 against the amplitude of the Halo orbit. As it can be noted, the costs are varying from a maximum of $2.94\,\mathrm{km/s}$ to a minimum of $\sim 1\,\mathrm{km/s}$, for a total transfer time always below $183\,\mathrm{days}$. The orders of magnitude obtained are consistent to what is found in the literature (see [14]), in which a slightly different method is employed that still connects a GEO with LEO using invariant manifolds.

A future extension to this work must analyse all the intersections between the manifolds and the Laplace plane. Here, only the intersection point closer to Earth was analysed, to limit the already long computation time due to the big number of parameters, but other solutions could deliver cheaper options. Furthermore, a similar analysis should be conducted for other periodic orbits that have been proposed for the future of Moon exploration, the already cited NRHOs, the Distant-Retrograde Orbits (DRO) and so on.

5.3 GSO - Graveyard orbit Connection

Here, we report the results obtained by following the procedure described in Section 4.3. Since the fact that the inclination of the GSO orbit is equal to $i = 7.4\,\mathrm{deg}$ and a manoeuvre changing the orbital plane is less probable in the final stage of the life of a space asset, given the costs involved, we assumed that the graveyard orbit has the same initial inclination of $7.4\,\mathrm{deg}$. We tested first the effectiveness of the IADC conditions by taking the initial eccentricity $e = 0.003$. The A/m parameter was let to vary from 0 to $1\,\mathrm{m^2/kg}$ and the perigee were computed using the Eq. (6). The initial angles were taken randomly. Fig. 19 and Fig. 20 show the minimum value of the radial distance and the maximum value of the radial distance reached over time. The purple horizontal lines are the edges of the GEO protected region, while the green line corresponds to the geostationary ring. These figures confirm that fulfilling the two IADC

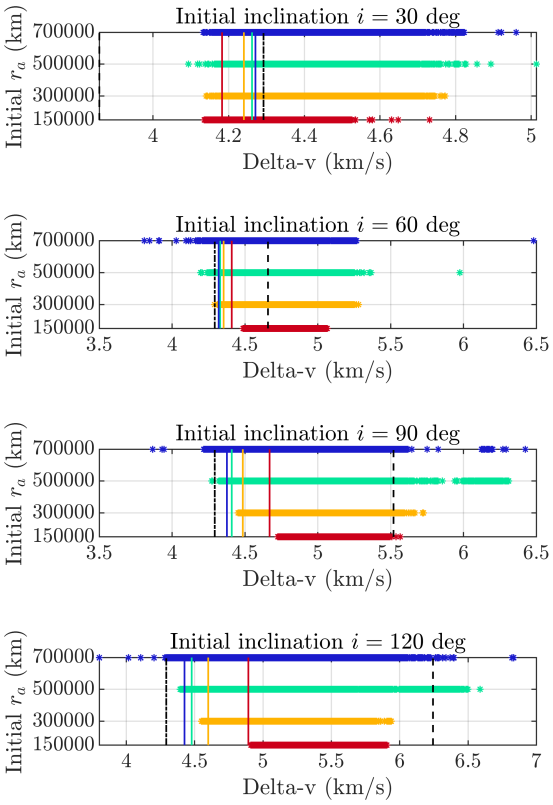

Fig. 13: Delta-v s against the radius of apogee of the first transfer orbit. Red, yellow, green and blue refer to r_a equal to 150 000 km, 300 000 km, 500 000 km, 700 000 km, respectively. The vertical dashed line is the two-impulses theoretical value, the dashed-dotted line is the theoretical limit of a bi-parabolic transfer. The solid coloured lines are bi-elliptic theoretical values, each colour is linked to the r_a of the transfer orbit and follows the previous colour-scheme: red for 150 000 km, yellow for 300 000 km etc.

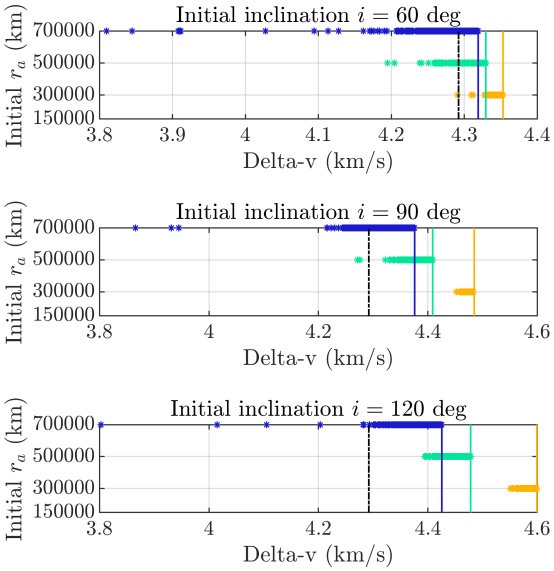

Fig. 14: Delta-v s against the radius of apogee of the first transfer orbit. Yellow, green and blue refer to r_a equal to 300 000 km, 500 000 km, 700 000 km, respectively. The dashed-dotted line is the theoretical limit of a bi-parabolic transfer. The solid coloured lines are bi-elliptic theoretical values.

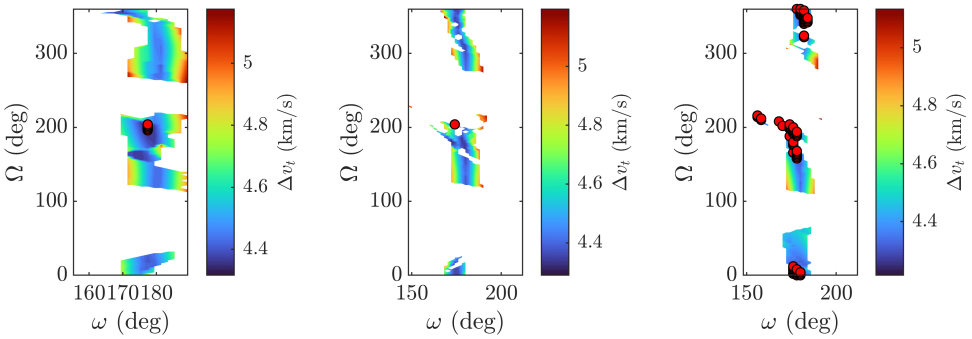

(a) Departure date $4/4/2023$.

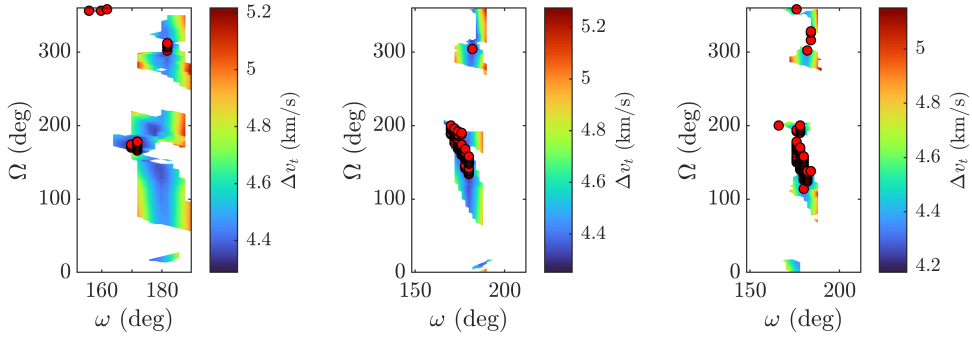

(b) Departure date $23/9/2023$.

Fig. 15: Delta-v maps for initial conditions $i_i = 60\,\text{deg}$, $r_{p,i} = 7500\,\text{km}$ and r_a = 300 000 km (left), r_a = 500 000 km (center), r_a = 700 000 km (right) and two different departure dates. The red dots represent the solutions that outperform the corresponding theoretical bi-elliptic transfers.

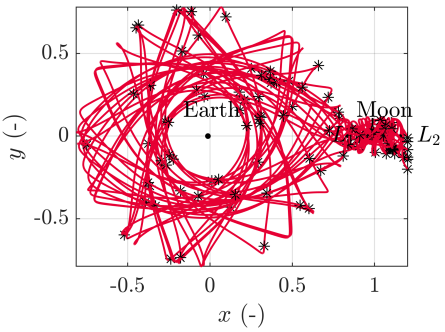

Fig. 16: $N = 10$ manifolds propagated for 6 months from a Halo with amplitude $A_z = 20\,000\,\mathrm{km}$. The stars represent the crossing points with the Laplace plane. The figure is represented in the CR3BP rotating frame.

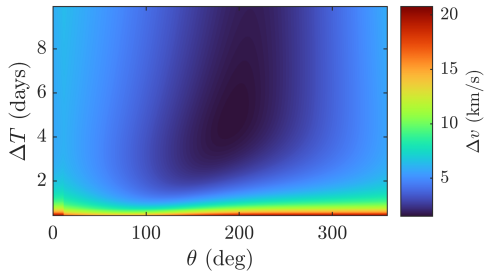

Fig. 17: Delta-v maps for the Lambert arc connecting a manifold with the target GSO, starting from a Halo with amplitude $Az = 10\,000\,\mathrm{km}$.

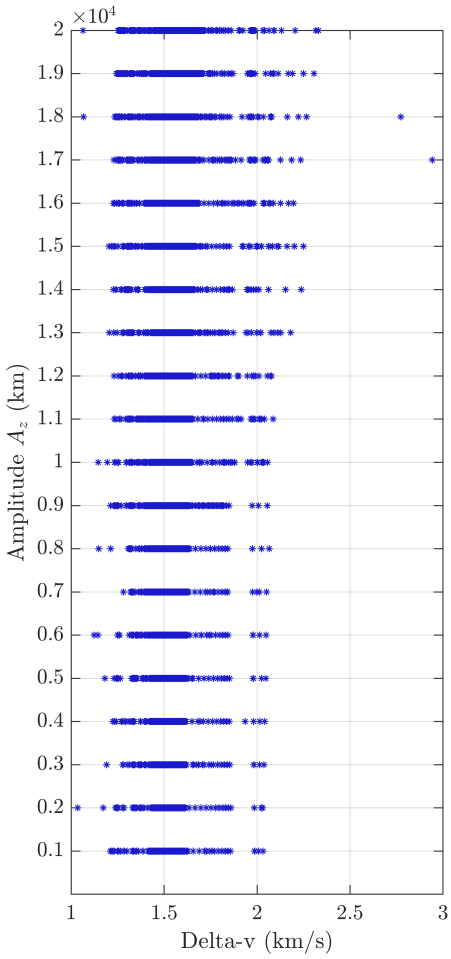

Fig. 18: Delta-vs for the Moon - GSO case for different Halo amplitudes.

conditions at the end of the disposal phase give orbits that remains above the GEO Protected Region for more than 100 years.

We explored other options. By enhancing the value of eccentricity, for instance to $e = 0.01$, we report in Fig. 21 similar results, but in this case, there are many orbits entering the GEO protected region, which suggest that the formula Eq. (6) is no longer valid, but could be adapted for slightly larger eccentricities.

6. Conclusions

In this paper, two different methods for performing a transfer from two orbital regimes to a circular GSO have been developed along with an analysis on the disposal orbits . The first method consists in connecting an orbit in LEO to the target GSO by exploiting the perturbations in the Earth's environment, in particular the third-body perturbations (from Sun and Moon). The proposed strategy consists in a four-impulse transfer, that requires raising the apogee of the first transfer orbit and then letting the perturbations act for a period of time, so that the total cost in terms of delta-v is lower than that of an ideal case, in which perturbations are not considered. By varying the initial parameters of the transfer orbit, such as inclination, apogee, departure date, RAAN and AOP, we can see how, for inclinations greater than a certain value (30 deg in this case) the proposed strategy outperforms the theoretical ones, like the direct two-impulses, bi-elliptical and bi-parabolic transfers. The limit of this approach is that the transfer time is considerably longer, and also it lacks the flexibility of choosing freely the initial conditions, such as the departure date. A future extension of this work will have to explore more initial parameters in order to obtain more general conclusions. The second method proposed in this paper concerns the connection of a Halo orbit around the L_2 point of Earth-Moon system to the circular GSO, using the invariant manifolds typical of the problem to approach the Earth, and then connect to the target orbit with a Lambert problem. By varying different parameters such as the amplitude of the Halo orbit, the time of flight on the arc and the entry point on the GSO, interesting solutions have been obtained in terms of delta-v and transfer time, that are comparable with the results in the literature that employ different transfer methods. In the future, this analysis should be expanded to other orbits of interest in the Earth-Moon system (such as NRHOs, DROs etc.). The third method deals with the analysis of disposal orbits, rather than with transfer methodologies. If for the first two cases, the focus is on exploiting those natural dynamical effects acting favorably on short/medium period of time, reducing thus the transfer costs, the third case identifies the regions of the phase space that lead to small variations of the orbital parameters, in particular of the eccentricity, on secular times. In the future, the analysis will be extended to other regions in the parameter space and to the modeling of on orbit fragmentation events.

Acknowledgement

This research was developed with the support of the ESA OSIP project "CORES: COllaborative REcycling of Solar power satellites". R.P. and C.G. acknowledge the support from the EU H2020 MSCA ETN Stardust-Reloaded, grant agreement no. 813644. We also thank Moritz Fontaine for his inputs throughout this work.

References

[1] Andrew Ross Wilson et al. "From life cycle assessment of space systems to environmental communication and reporting". In: *72nd International Astronautical Congress*. 2021, pp. 1–22.

[2] David Barnhart et al. "Phoenix program status-2013". In: *AIAA SPACE 2013 conference and exposition*. 2013, p. 5341.

[3] Aaron J Rosengren, Daniel J Scheeres, and Jay W McMahon. "The classical Laplace plane as a stable disposal orbit for geostationary satellites". In: *Advances in Space Research* 53.8 (2014), pp. 1219–1228.

[4] Ian McNally, Daniel Scheeres, and Gianmarco Radice. "Locating large solar power satellites in the geosynchronous Laplace plane". In: *Journal of Guidance, Control, and Dynamics* 38.3 (2015), pp. 489–505.

[5] Howard Curtis. *Orbital mechanics for engineering students*. Butterworth-Heinemann, 2013.

[6] BF Villac and DJ Scheeres. "New class of optimal plane change maneuvers". In: *Journal of guidance, control, and dynamics* 26.5 (2003), pp. 750–757.

[7] Stijn De Smet, Daniel J Scheeres, and Jeffrey S Parker. "Dynamics and stability of Sun-driven transfers from Low Earth to Geosynchronous Orbit". In: *Journal of Guidance, Control, and Dynamics* 41.9 (2018), pp. 2002–2010.

[8] William M. Kaula. *Theory of satellite geodesy. Applications of satellites to geodesy*. Blaisdell, Waltham, 1966.

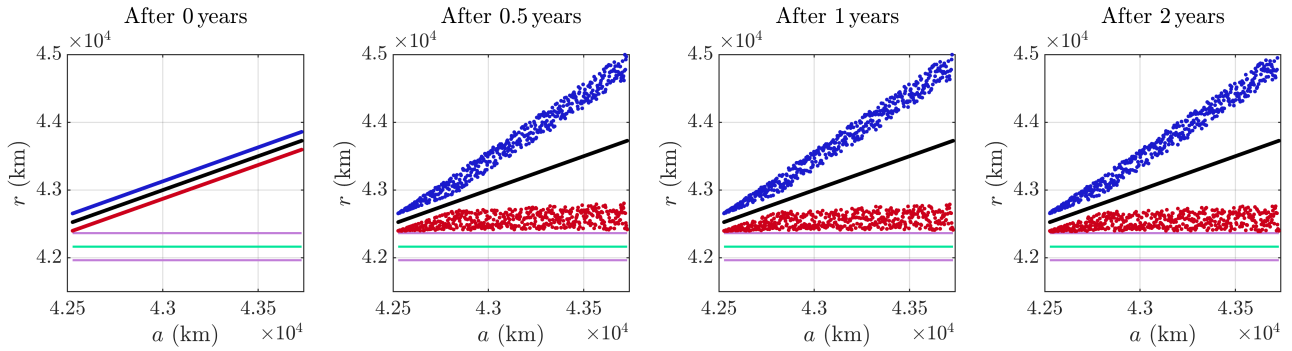

Fig. 19: Radial distance variation for 500 orbits characterized by the initial conditions $i = 7.4\,\mathrm{deg}$, $e = 0.003$, random values of the initial angles, r_p computed by using the formula (6) and $0 \leq A/m \leq 1\,\mathrm{m}^2/\mathrm{kg}$ (see the text for details). Each orbit is represented by three coloured points, marked in black, blue and red, where the black point gives the value of the semi-major axis, the red one provides the minimum perigee radius reached over the propagation time, while the blue point corresponds to the maximum apogee radius reached over the time span. The horizontal green line marks the location of the geostationary ring. The purple lines are the edges of the GEO protected region. Top left: $T = 0$, top right: $T = 0.5$ years, bottom left: $T = 1$ year, bottom right: $T = 2$ years.

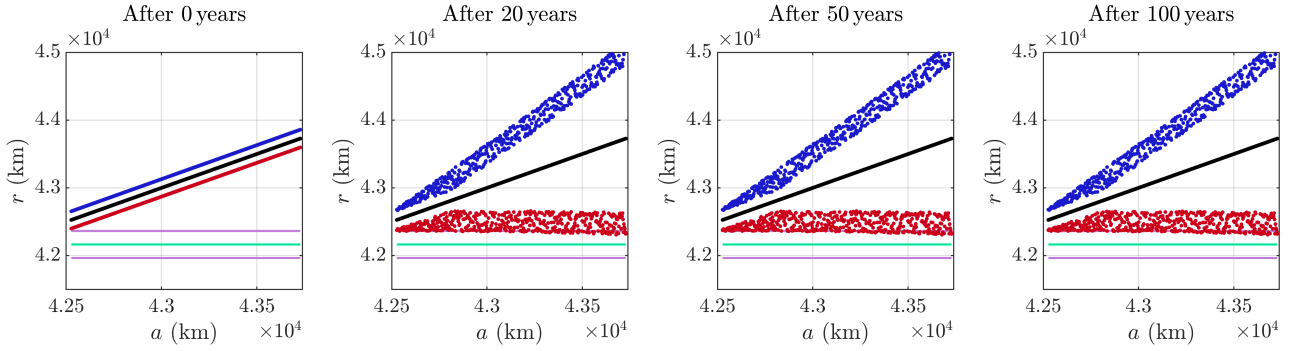

Fig. 20: Same as Fig. 19, but for $T = 20$ years (top right), $T = 50$ years (bottom left), $T = 100$ years (bottom right).

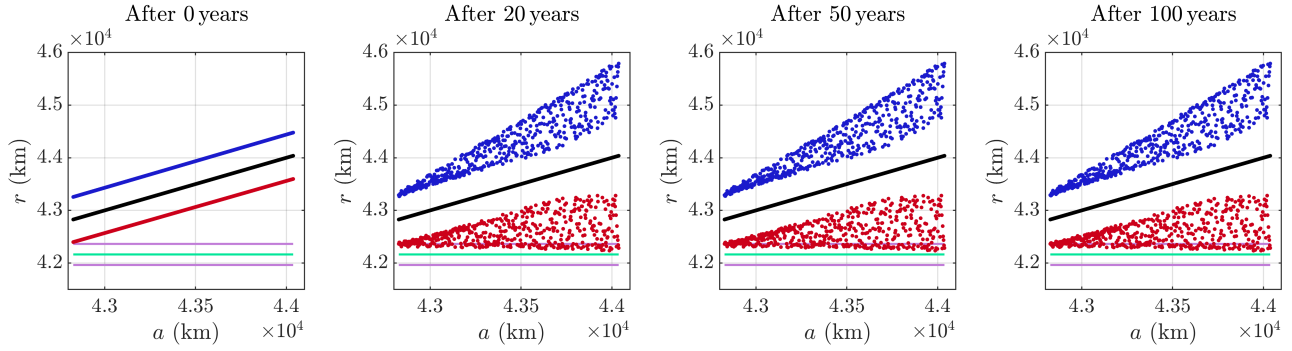

Fig. 21: Same as Fig. 20, but for $e = 0.01$.

[9] B Kaufman and R Dasenbrock. "Higher Order Theory for Long-Term Behavior of Earth and Lunar Orbiters". In: *NRL Repot 7527. Naval Research Laboratory*. 1972.

[10] M Misquero and C Galeş. "Accuracy and efficiency in the propagation of highly eccentric orbits". In: *Preprint* (2022).

[11] Diane C Davis et al. "Phase control and eclipse avoidance in near rectilinear halo orbits". In: *AAS Guidance, Navigation and Control Conference*. JSC-E-DAA-TN77422. 2020.

[12] E. Canalias et al. *Assessment of mission design including utilisation of libration points and weak stability boundaries*. Tech. rep. 03-4103a. Available on line at www.esa.int/act. European Space Agency, the Advanced Concepts Team, 2004.

[13] Bastien Le Bihan, Pierre Kokou, and Stéphanie Lizy-Destrez. "Computing an optimized trajectory between Earth and an EML2 halo orbit". In: (2014).

[14] F.B. Zazzera, F. Topputo, and M. Massari. *Assessment of mission design including utilisation of libration points and weak stability boundaries*. Tech. rep. 03-4103b. Available on line at www.esa.int/act. European Space Agency, the Advanced Concepts Team, 2004.

[15] Edward A Belbruno and James K Miller. "Sun-perturbed Earth-to-Moon transfers with ballistic capture". In: *Journal of Guidance, Control, and Dynamics* 16.4 (1993), pp. 770–775.

[16] Wang Sang Koon et al. "Dynamical systems, the three-body problem and space mission design". In: *Equadiff 99: (In 2 Volumes)*. World Scientific, 2000, pp. 1167–1181.

[17] Victor Szebehely and E Grebenikov. "Theory of Orbits-The Restricted Problem of Three Bodies." In: *Soviet Astronomy* 13 (1969), p. 364.

[18] Robert Willard Farquhar. *The utilization of halo orbits in advanced lunar operations*. Vol. 6365. National Aeronautics and Space Administration, 1971.

[19] E Canalias et al. "Assessment of mission design including utilization of libration points and weak stability boundaries". In: *ESA Advanced Concept Team* (2004).

[20] David L Richardson. "Analytic construction of periodic orbits about the collinear points". In: *Celestial mechanics* 22.3 (1980), pp. 241–253.

[21] Kathleen Connor Howell. "Three-dimensional, periodic,'halo'orbits". In: *Celestial mechanics* 32.1 (1984), pp. 53–71.

[22] Gerard Gomez et al. *Invariant manifolds, the spatial three-body problem and space mission design*. 109. American Astronautical Society, 2001.

[23] IADC-02-01 Revision 3. "IADC Space Debris Mitigation Guidelines". In: (2021). URL: https://www.iadc-home.org/documents_public/view/id/172%5C#u.

[24] Two-Line-Element catalogue. In: (2022). URL: https://celestrak.org/NORAD/elements/.

[25] S Hughes. "Earth satellite orbits with resonant lunisolar perturbations. I. Resonances dependent only on inclination". In: *Proc. R. Soc. Lond. A* **372**, *243-264* (1980).

[26] A Celletti, C Galeş, and G Pucacco. "Bifurcation of lunisolar secular resonances for space debris orbits". In: *SIAM J. Appl. Dyn. Syst.* **15**, *1352-1383* (2016).

[27] A Celletti, C Galeş, and C Lhotka. "Resonances in the Earth's space environment". In: *Comm. Nonlin. Sc. Num. Sim.* **84**, *105185* (2020).

[28] R R Allan and G E Cook. "The long-period motion of the plane of a distant circular orbit". In: *Proc. R. Soc. Lond. A* **280**, *97-109* (1964).

[29] Stéphane Valk et al. "Global dynamics of high area-to-mass ratios GEO space debris by means of the MEGNO indicator". In: *Advances in Space Research* 43.10 (2009), pp. 1509–1526.

[30] Marilena Di Carlo, Massimiliano Vasile, and Stephen Kemble. "Optimised GTO-GEO transfer using low-thrust propulsion". In: *31st International Symposium on Space Technology and Science (ISTS)*. 2017.

[31] Ralph B Roncoli. "Lunar constants and models document". In: *JPL D-32296, Sept* (2005).